Enhancing the Performance of the Multi-Order Probabilistic Approach in Angular Speed Estimation through Adaptive Window Selection

Georgios Protopapadakis, Cédric Peeters, Quentin Leclère, Jan Helsen

Enhancing the Performance of the Multi-Order Probabilistic Approach in Angular Speed Estimation through Adaptive Window Selection

Georgios PROTOPAPADAKIS[1], Cédric PEETERS[1], Quentin LECLERE[2] and Jan HELSEN[1]

[1] Department of Applied Mechanics, Vrije Universiteit Brussel Belgium
[2] Univ Lyon, INSA-Lyon, LVA, EA677, F-69621 Villeurbanne, France
georgios.eftichios.protopapadakis@vub.be

Abstract

The Multi-Order Probabilistic Approach (MOPA) is a method for estimating the instantaneous angular speed from vibration signals with high precision. However, determining the optimal choice of inputs can be challenging as the method requires many input parameters, including the window size selection used to generate the spectrogram for computing the probability density functions. This study presents a new approach that utilises statistical indicators to evaluate the information content of various window sizes and selects the optimal size for each signal segment. The algorithm is tested using simulated sensor data and real data from offshore wind turbines, and the results are compared to benchmark parameters such as the Root Mean Squared Error (RMSE). The results show that the proposed approach provides similar accuracy in estimating angular speed without the necessity to pre-select a window size for the spectrogram. Overall, this study demonstrates that using an adaptive window based on statistical indicators can improve the flexibility of MOPA as well as reduce the time required to detect the appropriate window for each data set.

1 Introduction

Monitoring plays a pivotal role in various applications, especially in the domain of rotating machinery such as wind turbines. Vibration monitoring is widely recognised as one of the primary methods employed for this purpose. Spectral analysis methods are typically used to identify faults occurring in the rotating components of the machinery, including the gearbox, bearings, and shafts. However, a significant challenge arises due to the variable operating conditions of rotating machines, resulting in a phenomenon known as peak smearing. To mitigate this issue, signal resampling is employed, necessitating the knowledge of the Instantaneous Angular Speed (IAS).

IAS can be obtained through various means, such as rotary encoders or visual trackers. However, these approaches often prove to be expensive or impractical in certain scenarios. As an alternative, indirect methods based on vibration analysis have been explored, including techniques such as the Hilbert transform [1], Bayesian estimation [2], and the inaction method [3]. Despite their potential, these methods encounter several challenges, as highlighted in previous research [4]. These challenges include dealing with a low signal-to-noise ratio, the presence of multiple harmonics in the signal, and the interaction between rotation harmonics and the machine's structural resonance. Several other methods, such as Phase Demodulation, Iterative Phase Demodulation [5], Multi-Order Probabilistic Approach (MOPA) [6], Teager Kaiser Energy Operator (TKEO) [7], ViBES [8], and Maximum tracking in combination with a Vold-Kalman filter [9], have been proposed. In a comprehensive review of these methods, Peeters et al. conclude that each approach has its own advantages and limitations, resulting in varying levels of applicability and accuracy [8]. Notably, vibration data typically exhibit multiple harmonics rather than a single dominant frequency. Methods capable of converging on multiple harmonics are particularly valuable. According to Peng et al., MOPA appears to be one of the most accurate methods, with the possibility of Phase Demodulation being more accurate when harmonics have a high signal-to-noise ratio throughout the entire record [10]. A Multi-harmonic Phase Demodulation method was developed to achieve high precision by combining the benefits of MOPA - multiple harmonics - and the accuracy of phase

demodulation when the harmonic with the highest signal-to-noise ratio is identified [11]. However, the use of Multi-harmonic Phase Demodulation requires knowledge of the initial speed, which adds complexity to the process. Hence, this paper focuses on estimating IAS using the MOPA method [6]. MOPA is capable of tracking harmonics in a Time-Frequency Representation (TFR) of the vibration signal, which can vary in complexity. However, the effectiveness of MOPA heavily relies on the quality of the TFR, suggesting the potential for enhancing speed estimation by improving the TFR's quality. Nevertheless, generating a high-quality TFR can be challenging, resulting in noisy speed estimations or incorrect convergence of MOPA on the wrong harmonic.

Akan et al. described the various methods for generating a TFR [12]. Time-Frequency Distributions is the first category, including the Short-Time Fourier Transform (STFT) in the linear case [13], and Cohen's bilinears such as the Wigner-Ville transform [14]. Additionally, Wavelet transforms [15], Time-Frequency Atomic Decompositions (with the Gabor expansion [16] being the most well-known), and data-adaptive mode decomposition methods are commonly employed [12]. However, many of these methods can be computationally expensive, require careful parameter optimisation, or involve conceptual intricacies due to unclear relationships and kernel functions. Among the different methodologies, STFT is the most widely used and understandable TFR. Therefore, this work focuses on producing an STFT that minimises the MOPA speed estimation error while reducing user intervention.

The main challenge with STFT is the inherent tradeoff between time and frequency resolution, as dictated by the Heisenberg-Gabor uncertainty principle [17]. In other words, the selection of the window always involves a compromise between time and frequency resolution. For instance, using small windows provides a good time resolution but comes at the cost of a worse frequency resolution. This problem becomes even more complex for rotating machinery, where the machine's speed varies with time.

To address this issue, several attempts have been made. One well-known method is the Synchrosqueezing transform (SST) [18]. SST is an invertible transformation that utilises instantaneous frequency to sharpen the spectrogram representation by maximising energy and reducing the bandwidth of harmonics. This method has seen advancements such as Synchroextracting transform and others [19]. However, according to Iatsenko et al., synchrosqueezing may enhance visual representation but does not provide actual better resolution in terms of amplitude/frequency variations [20]. Another method employed to improve the quality and interpretability of STFT is the adaptive window. One of the earliest attempts was made by Jones and Baraniuk, who used sparsity indices to determine the window that favours a more "peaky" distribution [21]. Building on this work, Czerwinski and Jones proposed the Cone length to reduce computation requirements [22]. In a more recent study, Zhong et al. obtained the Instantaneous Frequency by following the ridge of the wavelet transform and used its gradient to define the window size [23]. Further advancements involve minimising or maximising specific criteria, an updated version of Jones' approach [24, 25]. Additionally, a differentiable STFT with adaptive windows is proposed using the Shannon entropy as an optimisation criterion [26].

Previous research has emphasised the potential visual enhancements of an adaptive window STFT, yet failed to investigate its practical implications in real-world scenarios. Therefore, this study seeks to bridge this gap by implementing an adaptive window spectrogram and examining its direct impact on precise IAS estimation using MOPA.

2 Proposed Method

This section presents the proposed method, starting with the introduction of the MOPA method. It then proceeds to discuss the STFT, the modifications made to it, and finally, the definition of the indicator used for window selection.

2.1 Multi-Order Probabilistic Approach

MOPA is tracking the harmonics directly from the TFR [6]. This is done by computing the probability density function of the speed of the rotating component ω (in Hz). A range of speed $(\Omega_{min}, \Omega_{max})$ needs to be given, in order to define the region that the pdf needs to be calculated. Where the pdf has a high probability - the TFR has high amplitude - it is the most likely that this frequency is the velocity of the rotating part.

$$\begin{cases} p(\Omega|H) = \frac{1}{\xi} A(H\omega) & \text{for } \Omega_{min} < \omega < \Omega_{max} \\ p(\Omega|H) = 0 & \text{elsewhere} \end{cases} \tag{1}$$

Where p is the density function of the IAS Ω, $A(H\omega)$ is the spectrum for the given frequency ω. H is the order of the excitation that is understudy (e.g. $H = 1$ if it is the first harmonic of the understudy shaft). ξ is a normalisation factor that is given:

$$\xi = \int_{\Omega_{min}}^{\Omega_{max}} A(H\omega)\, d\omega \tag{2}$$

Since these pdfs need to be computed independently for all windows of the TFR, discontinuities might be present, that are not existing in velocities of real-life scenarios. For that reason, continuity is applied by taking into account not only the in question timestep but also neighbouring ones. This is performed by convolving using a centered Gaussian with $\sigma_k = \gamma k \Delta t$ and Δt being the time step, γ being the standard acceleration of the IAS. The pdf including continuity, is defined as:

$$p(\Omega_j)_{j+k} = \int_{\Omega_{min}}^{\Omega_{max}} p(\Omega_j|\Omega_{j+k})\, d\omega \propto e^{\frac{\omega^2}{2\sigma_k^2}} * p(\Omega_{j+k}) \tag{3}$$

To account for multiple orders of the baseline harmonic, that be higher harmonics of the same component or maybe other harmonics from other coupled components, H must be a vector of length L with all the understudy orders. Then the pdfs need to be multiplied in order to get the final speed estimation, based on the estimation of the pdf from all orders:

$$p(\Omega_j)_s \propto \prod_{i=-K}^{K} [\Omega_j]_{j+i} \tag{4}$$

with K being $L/2$.

2.2 Adaptive window STFT derivation

The Fourier transform is given by:

$$\hat{X}(f) = \int_R x(\tau) e^{-j2\pi f \tau}\, d\tau \tag{5}$$

with f the frequency.

For a signal $x(\tau)$ with a finite number of samples N, then the discrete Fast Fourier Transform (FFT) can be written:

$$\hat{X}[k] = \sum_{n=0}^{N-1} x[n] e^{-j2\pi k \frac{n}{N}} \tag{6}$$

with k being the Fourier index and $0 \leq k \leq N-1$.

The windowed version of the continuous FFT, the STFT, for an infinite-length signal, is given to be:

$$X(t,f) = \int_R x(t+\tau) w(\tau) e^{-j\omega\tau}\, d\tau \tag{7}$$

with t the time, $w(\tau)$ is the window that is used to define the length and location of the segment of the signal to be studied, as well as potential tapering. For the discrete, in time and frequency, case of a finite signal, the equation (7) can be transformed into the following:

$$X[t,k] = \sum_{n=0}^{N-1} x[t+n] w[n] e^{-j2\pi k \frac{n}{N}} \tag{8}$$

where t and k denote the starting time point for the localised Fourier Transform and Fourier index accordingly (again $0 \leq k \leq N-1$). N defines again the length of the discrete Fourier Transformation, while the variable n is

employed to denote the specific point (sample index) of the extracted segment from the original time function using the window $w[n]$. In other words, the algorithm computes for each segment of signal starting at time t an FFT of length N, using a window w that defines the tapering. By applying this process to multiple time steps, a spectrogram is generated. The step in time defines also the overlapping of data, which is often used for better accuracy.

As mentioned earlier, the objective of this study is to implement an adaptive window STFT. The aim is to dynamically update the window length for each timestep, t, based on a chosen indicator. To achieve this, the variable N, which determines the number of samples (FFT length), needs to be time-dependent. However, this approach results in spectrogram segments with varying time and frequency resolutions. To address this issue, zero-padding is applied to the signal segment, allowing N to remain constant and mitigating the resolution discrepancies. The signal used for each window can be defined by Equation 9:

$$\vec{x} = [\underbrace{0 \cdots 0 \ \overbrace{x[t] \cdots x[t+M(t)]}^{\text{variable length } M(t)} \ 0 \cdots 0}_{\text{constant length } N}] \tag{9}$$

where $M(t)$ represents the segment length, determined by the indicator, that is then subjected to zero padding. This ensures that the frequency resolution remains consistent and facilitates the utilisation of the Time-Frequency Representation (TFR) with MOPA.

2.3 Indicators

To determine an appropriate window size, an indicator is utilised in an iterative manner for each signal segment. As previously explained, MOPA calculates the probability density of the speed along the time axis, with higher accuracy achieved when the TFR representation exhibits more pronounced harmonics.

Peak smearing can occur in the spectrum when there is acceleration (positive or negative) in the rotating machine, as the harmonics do not maintain a constant frequency. Different segments may require varying optimal window sizes depending on the level of acceleration. Typically, the window that exhibits the highest sparsity in the spectrum, indicating a concentrated spectral density at a specific frequency, is considered favourable. Therefore, indicators such as the L_1 norm, which assesses sparsity, can effectively determine the window with the most pronounced frequency peak. When acceleration is present, the indicator tends to favour smaller windows to minimise peak smearing, whereas in the absence of acceleration, larger windows are preferred for improved frequency resolution.

The primary indicator employed in this study is the Hoyer index. Based on Hurley and Rickard's research, the Hoyer index is regarded as one of the most accurate measures of sparsity, surpassed only by the Gini index [27]. However, the Gini index requires the spectrum values to be sorted, making it computationally intensive. Note that $L_p = (\sum \hat{X}^p)^{1/p}$ with $\hat{X}$ being the result of the FFT, so that the Hoyer index is given below:

$$Hoyer = \frac{\sqrt{N} - \frac{L_1}{L_2}}{\sqrt{N} - 1} \tag{10}$$

3 Test cases and results

In order to check the efficiency of Adaptive Short Time Fourier Transform specifically for the application with MOPA and speed estimation, two main tests were conducted. First, a simulated signal was created in order to verify the assumption of the sparsity index. Then the adaptive window STFT was tested on the CMMNO14 data [6].

3.1 Simulated data

3.1.1 Signal generation

To generate the simulated signal, the following steps were executed. Firstly, a shaft was created with a predefined IAS profile, which follows a sinusoidal pattern. The IAS profile was mathematically defined by Equation 11:

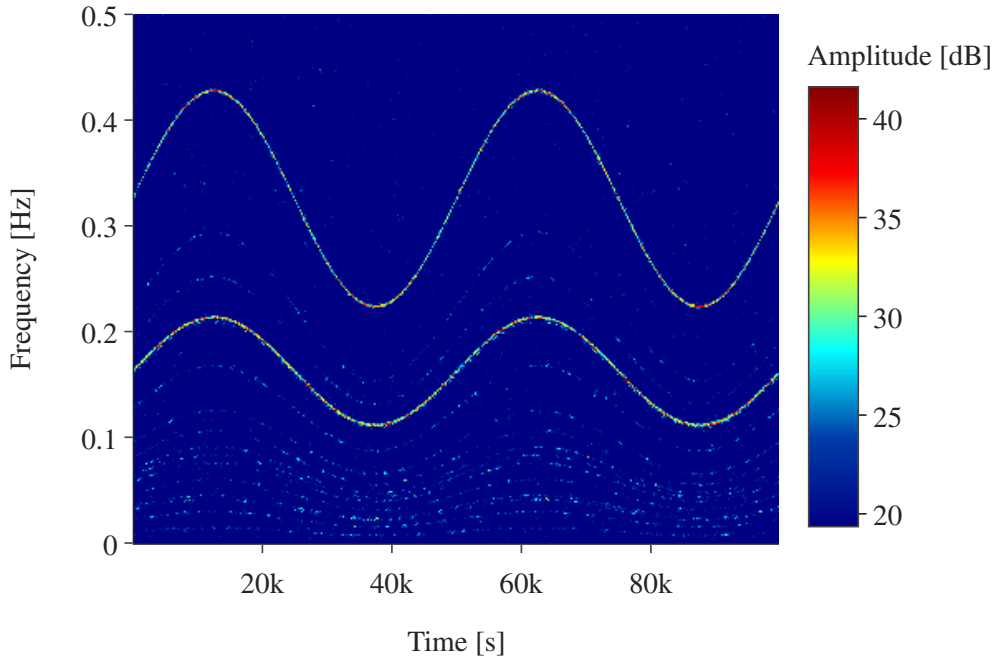

Figure 1: SPECTROGRAM OF THE SIMULATED SIGNAL (WINDOW = 450, OVERLAP = 95%, NFFT = 4096)

$$V(t) = V_0 + a_1 sin(2\pi f_u t) \tag{11}$$

where a_1 defines the amplitude of the first harmonic, f_u is the fundamental frequency (decided such that the signal has two periods T). V_0 is the offset that defines the mean value and makes sure that the IAS is always positive. For the case that is demonstrated later in the results, the values are selected to be: $a_1 = 0.01$, $V_0 = 0.032$, $f_u = 2e^{-5}$ such that for a signal of a duration of $t_{total} = 100000$ seconds, the period $T = t_{total}/2$. Note that the acquisition frequency F_s for this particular example is selected to be 1 Hz.

In order to replicate a more realistic signal, additional harmonics were added to the signal. Six harmonics were included, and Gaussian noise was applied ($\mu = 0$ and $\sigma^2 = 0.1$). Considering that the maximum amplitude of the signal is defined as 1, then $\sigma^2 = 0.1$ corresponds to a signal-to-noise ratio (SNR) of 20. Moreover, two harmonics representing a planetary gearbox with a gear ratio of 0.3636 and a meshing order of 5.091 were incorporated into the signal, along with corresponding noise. Lastly, a second shaft rotating at 0.3636 times the speed of the first shaft was included, accompanied by noise and seven harmonics.

The resulting spectrogram of the simulated signal is depicted in Figure 1. Notably, the harmonics of the gearbox are prominently visible in the spectrogram, exhibiting stronger magnitudes compared to the shafts.

3.1.2 Results

The setup of the adaptive window STFT, MOPA and the parameters of the baseline spectrogram are presented in table 1:

Adaptive Window	Base spectrogram	MOPA
N_w: (64 - 1536, 16)	N_w: (64 - 2048, 128)	H_i: [0.36, 1, 5.09]
Δt: 20	Δt: N_w*0.05	k_w: 15
Hann window	Hann window	γ: 1
$NFFT$: 4096	$NFFT$: 4096	ω_{min}: 0.022 Hz
		ω_{max}: 0.042 Hz

Table 1: SETUP PARAMETERS AND THEIR RANGE FOR THE SIMULATED CASE

where F_s is the signal acquisition frequency, N_w the window used (in this case it is a range), Δt the step in time of the spectrogram (depends on the overlap), $NFFT$ is the FFT size. ω_{min} and ω_{max} are the minimum and maximum expected speed, γ is the expected acceleration, k_w is the number of windows used for continuity and H_i is the list of orders that are taken into account in MOPA. Note that two harmonics per order are considered.

Figure 2 displays the speed estimation (red) in close proximity to the actual speed (black), indicating a high degree of accuracy. The associated window sizes are shown in blue. Remarkably, at each vertex of the parabolic shape, where acceleration is reduced, the window tends to increase in size, whereas, during periods of significant acceleration, the window size decreases. Figure 3 provides a visualisation of the actual window sizes relative to the absolute acceleration, thereby affirming the hypothesis put forth in Section 2.3 regarding the

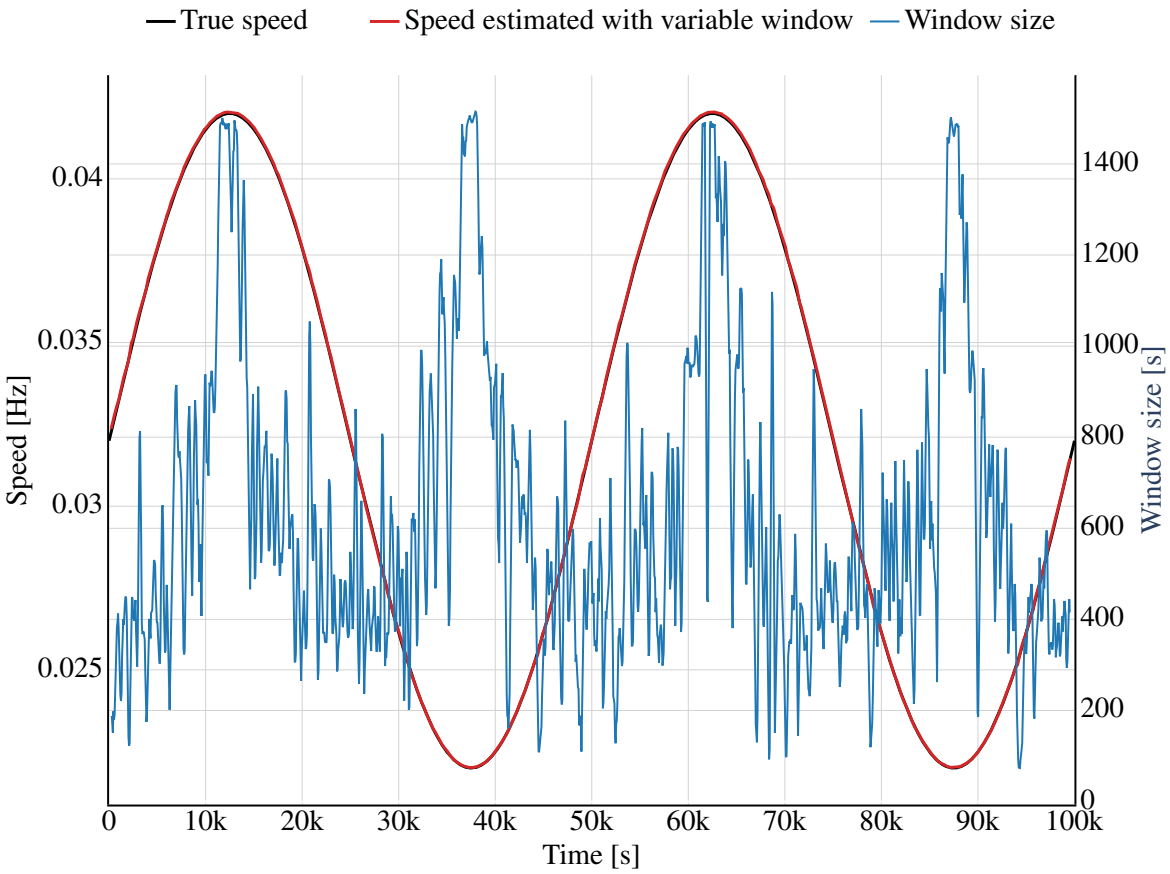

Figure 2: SPEED ESTIMATION AND WINDOW SIZE RESULTS

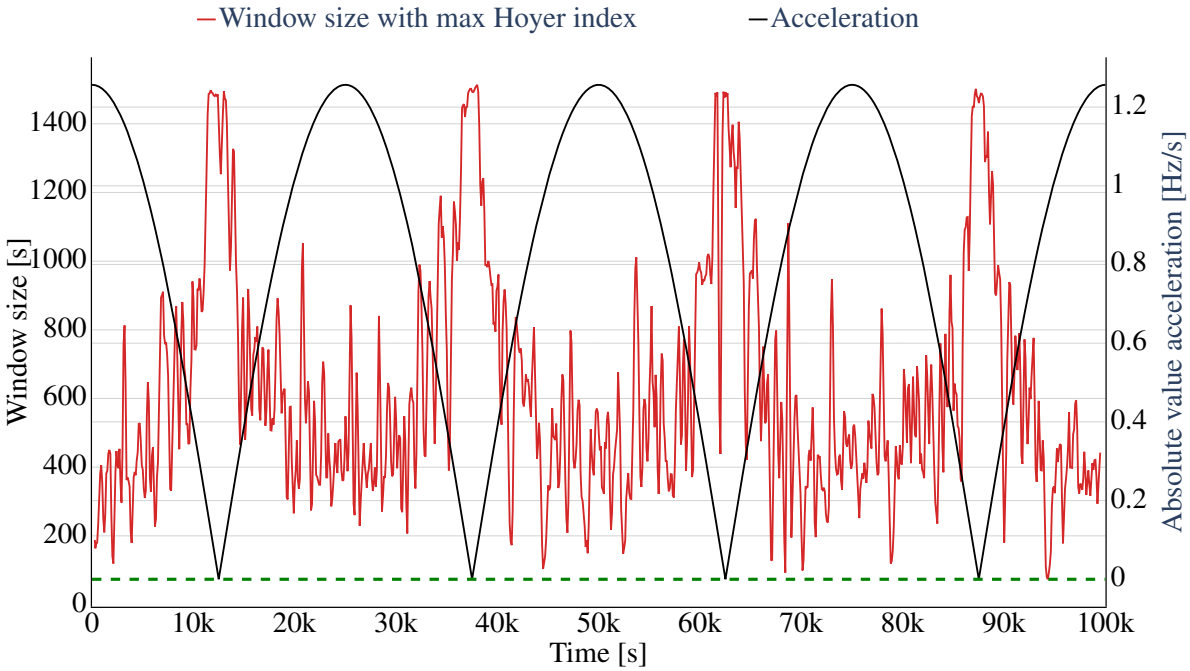

Figure 3: WINDOW SIZE (MAX HOYER) AGAINST ACCELERATION

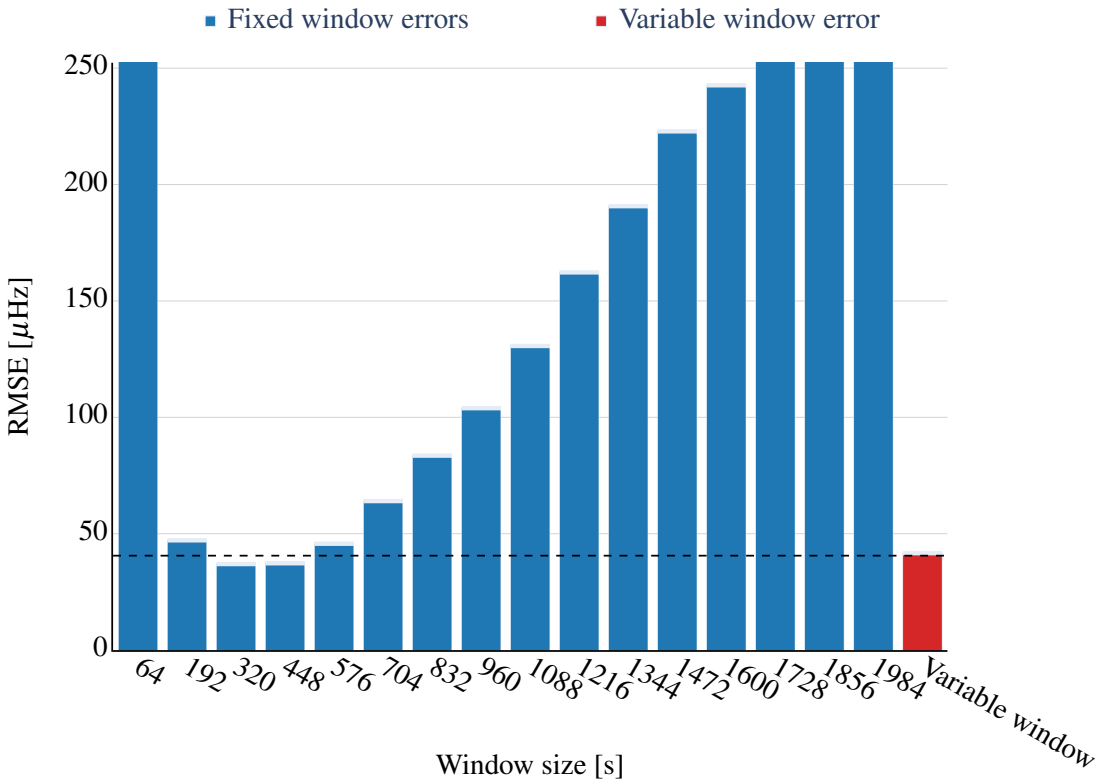

Figure 4: RMSE ERROR PER WINDOW SIZE AGAINST ADAPTIVE WINDOW

relationship between sparsity and speed variation. The green line in the figure emphasises the zero acceleration boundary.

To evaluate the accuracy of this method compared to a typical spectrogram, various spectrograms with different window sizes were tested, as outlined in Table 1. The results presented in Figure 4 demonstrate that the accuracy of MOPA, when applied in conjunction with the adaptive window spectrogram, is nearly equivalent to that achieved with an optimal constant window. This finding is highly promising, especially considering that the simulated signal is relatively straightforward with no significant variations in behaviour. Moreover, the automatic selection of an optimal or near-optimal spectrogram by simply defining a window range not only achieves good accuracy but also reduces the required post-processing time for the signal.

3.2 CMMNO 2014 dataset

The CMMNO 2014 dataset includes a vibration signal of a wind turbine gearbox. The duration of the signal is 547 seconds and the acquisition frequency is 5 kHz. More information about the dataset can be found in previous works [6, 8].

3.2.1 Results

The configuration details of the adaptive window STFT, MOPA, and the parameters used for the baseline spectrogram in the CMMNO case are summarised in Table 2. For this particular case, the selection was made to utilise three harmonics of the first two orders (H_i), along with two harmonics from the remaining orders.

Adaptive Window	Base spectrogram	MOPA
N_w: (1500 - 15000, 128)	N_w: (500 - 14500, 1000)	H_i: [1, 5.3, 26, 29]
Δt: 750	Δt: N_w*0.2	k_w: 10
Rectangular window	Rectangular window	γ : 0.4
$NFFT$: 20000	$NFFT$: 20000	ω_{min}: 18 Hz
		ω_{max}: 30 Hz

Table 2: SETUP PARAMETERS AND THEIR RANGE FOR THE CMMNO CASE

Figure 5 presents a comparison between the estimated and the actual IAS. Notably, the estimated IAS demonstrates smoothness, particularly considering that only 10 windows were involved in the convolution process. The tendency of the window size to increase in regions where the speed remains constant or exhibits relatively small acceleration is further depicted in Figure 6.

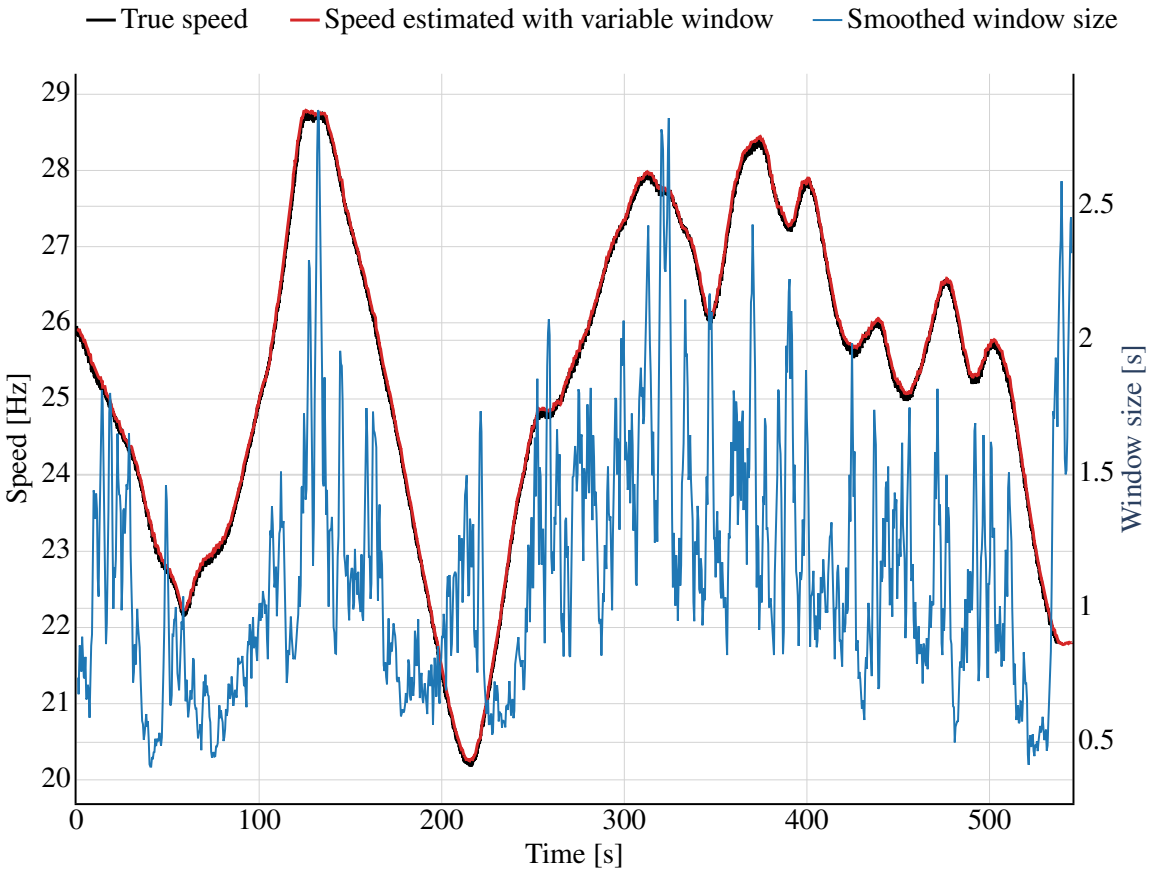

Figure 5: SPEED ESTIMATION AND WINDOW SIZE RESULTS

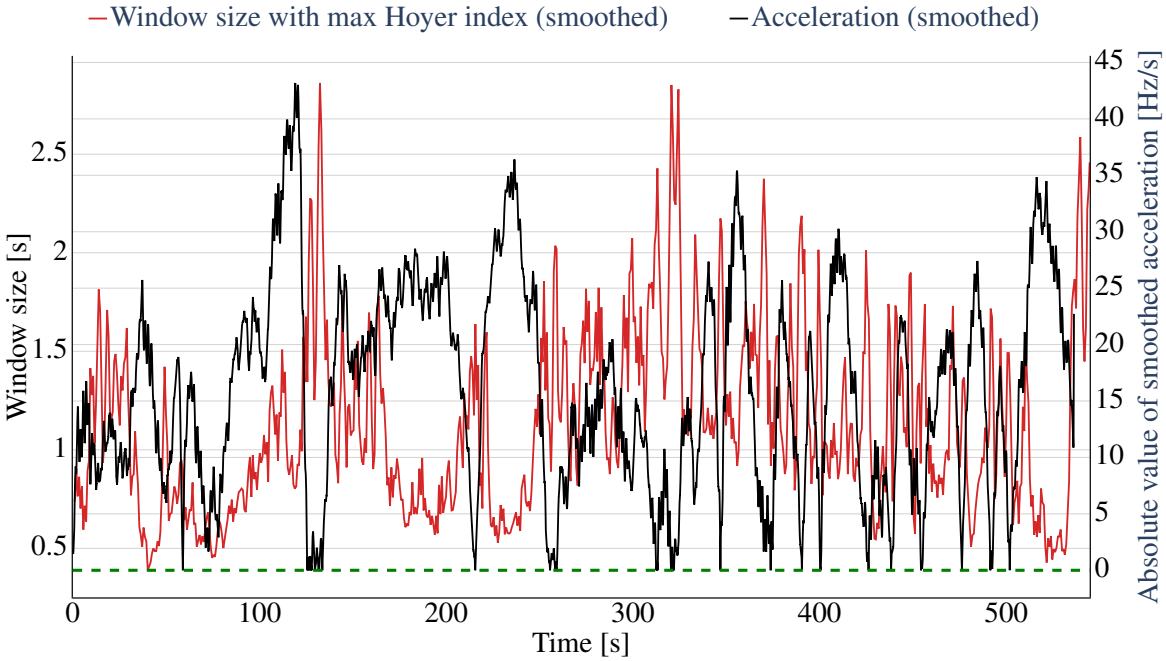

Figure 6: WINDOW SIZE (MAX HOYER) AGAINST ACCELERATION

Once again, the adaptive window spectrogram yields favourable results, exhibiting accuracy comparable to

that achieved with the optimal window, as illustrated in Figure 7. It is worth noting that the Hoyer index may be influenced by harmonics present in the signal but not utilised in the speed estimation. Nonetheless, these findings are highly promising, indicating the method's remarkable precision. With further advancements and refinements, there is strong potential for the method to significantly surpass the performance of the standard approach.

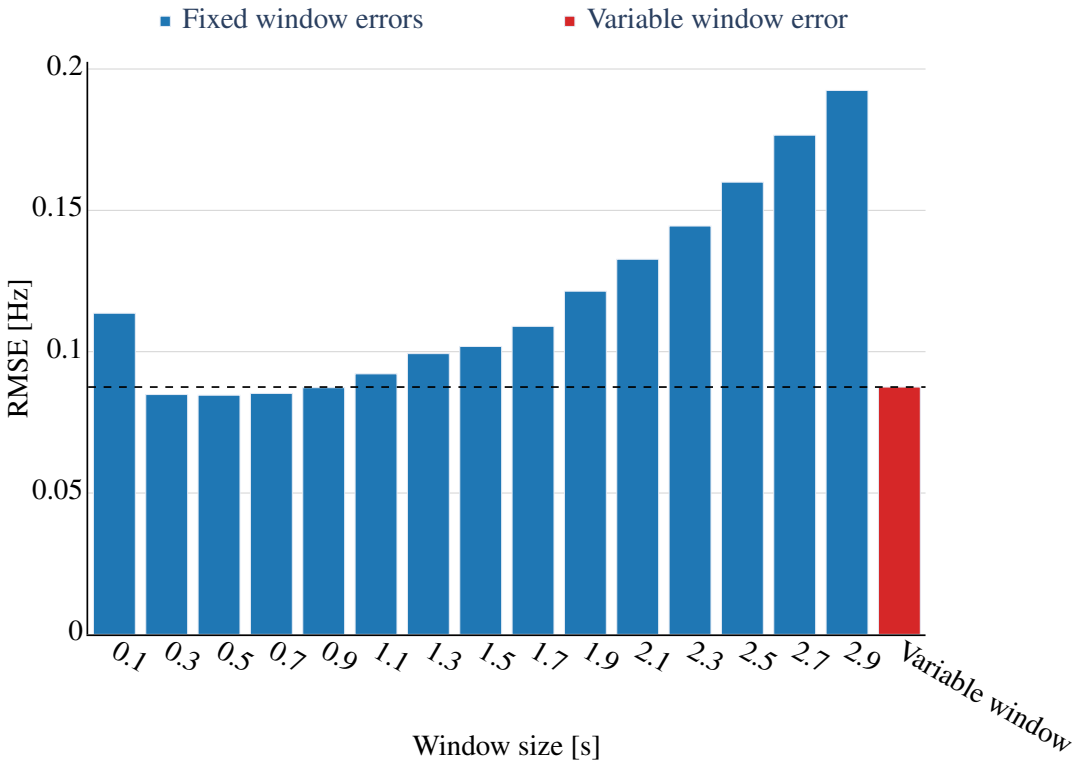

Figure 7: RMSE ERROR PER WINDOW SIZE AGAINST ADAPTIVE WINDOW

3.3 Discussion

Currently, the adaptive window spectrogram offers the significant advantage of a more simplified deployment, eliminating the need to manually select a specific window size and instead focusing on a window range. The proposed automatic approach demonstrates an impressive ability to achieve a high level of accuracy, even without prior knowledge of the true IAS. In practical scenarios, it is often challenging to determine the true IAS, which in turn makes it difficult to identify the optimal fixed window size based on the estimated IAS. However, this paper provides compelling evidence that the proposed adaptive scheme effectively approximates the attainable optimal accuracy, despite not having access to the true IAS information. This significant finding showcases the robustness and reliability of the adaptive window spectrogram, as it consistently achieves results that are comparable to the accuracy achieved with the optimal window size, even in the absence of knowledge about the true IAS.

To further enhance the methodology, a variable step in time (overlap) could be implemented. This would enable more significant time steps when utilising larger windows, indicating lower acceleration values. Similarly, smaller steps in time would be more suitable for detecting acceleration in situations where smaller windows are employed.

One limitation of the iterative approach is the computational time required, which surpasses that of a typical spectrogram by an order of magnitude. The computational demand of the adaptive window spectrogram is mainly dependent on the number of windows being tested. Importantly, the time needed to generate the adaptive spectrogram is considerably shorter compared to that required for a single MOPA execution. As a result, if a significant number of fixed windows need to be tested in conjunction with MOPA to identify the optimal IAS estimation, the process would be significantly more time-consuming compared to the adaptive spectrogram approach. In the future, alternative approaches could be explored, such as gradient-based optimisation or physics-informed decision-making, tailored to specific applications. Additionally, potential improvements in

accuracy could be achieved by employing different sparsity indices or optimisation functions.

Considering that MOPA functions as a multi-harmonic speed estimator, optimising the spectrogram on a per-frequency bin basis is an intriguing avenue to explore. Given the substantial difference in frequency between lower and higher harmonics, determining the optimal window for each frequency bin could potentially enhance accuracy across the entire frequency range.

To validate the effectiveness of the adaptive window spectrogram in real-life scenarios, future work should involve conducting tests using vibration data obtained from operating wind turbines. This will provide valuable insights into the efficiency and applicability of the method under practical conditions.

4 Conclusions

In this study, an adaptive window spectrogram was developed for the purpose of speed estimation in rotating machines when used in conjunction with MOPA. The fundamental concept behind this approach was to identify an optimal window for assessing the spectral density of the signal under different operating conditions. Each signal segment was subjected to iterative testing with various windows, and the window with the highest Hoyer index was selected.

To evaluate the effectiveness of the method, both a simulated signal and CMMNO 2014 data were utilised. The proposed adaptive window spectrogram demonstrates accuracy on par with the optimal fixed window size, without relying on knowledge of the true IAS. This highlights the robustness and practicality of the method, making it a promising and valuable tool for speed estimation in rotating machines. Furthermore, by employing the adaptive window approach, the need for time-consuming manual selection of the optimal window for each machine is eliminated, albeit at the cost of slightly slower spectrogram generation.

Moreover, the inherent physical connection between window selection and the acceleration of the rotating machine lends credence to the adoption of this methodology. Future enhancements could potentially refine the adaptive window spectrogram and elevate its performance even further. Taken together, the findings from this study provide evidence supporting the benefits and justification for implementing an adaptive window spectrogram.

References

[1] M. Zhao, J. Lin, X. Xu, and Y. Lei. Tacholess envelope order analysis and its application to fault detection of rolling element bearings with varying speeds. *Sensors*, 13(8):10856–10875, 2013. ISSN 1424-8220. doi: 10.3390/s130810856.

[2] Y. Hu, F. Cui, X. Tu, and F. Li. Bayesian estimation of instantaneous speed for rotating machinery fault diagnosis. *IEEE Transactions on Industrial Electronics*, 68(9):8842–8852, 2021. doi: 10.1109/TIE.2020.3013526.

[3] L. Gu, Q. Tian, and Z. Ma. Extraction of the instantaneous speed fluctuation based on normal time–frequency transform for hydraulic system. *Proceedings of the Institution of Mechanical Engineers, Part C: Journal of Mechanical Engineering Science*, 234(6):1196–1211, 2020. doi: 10.1177/0954406219891187.

[4] X. Yu, Z. Feng, and D. Zhang. Adaptive high-resolution order spectrum for complex signal analysis of rotating machinery: Principle and applications. *Mechanical Systems and Signal Processing*, 177:109194, 2022. ISSN 0888-3270. doi: 10.1016/j.ymssp.2022.109194.

[5] M. D. Coats and R. Randall. Order-tracking with and without a tacho signal for gear fault diagnostics. 2012.

[6] Q. Leclère, H. André, and J. Antoni. A multi-order probabilistic approach for instantaneous angular speed tracking debriefing of the cmmno14 diagnosis contest. *Mechanical Systems and Signal Processing*, 81: 375–386, 2016. ISSN 0888-3270. doi: 10.1016/j.ymssp.2016.02.053.

[7] Robert Randall and Wade Smith. Use of the teager kaiser energy operator to estimate machine speed. In *PHM Society European Conference*, volume 3, 2016.

[8] C. Peeters, Q. Leclère, J. Antoni, P. Lindahl, J. Donnal, S. Leeb, and J. Helsen. Review and comparison

of tacholess instantaneous speed estimation methods on experimental vibration data. *Mechanical Systems and Signal Processing*, 129:407–436, 2019. ISSN 0888-3270. doi: 10.1016/j.ymssp.2019.02.031.

[9] S. Schmidt, P.S. Heyns, and J.P. de Villiers. A tacholess order tracking methodology based on a probabilistic approach to incorporate angular acceleration information into the maxima tracking process. *Mechanical Systems and Signal Processing*, 100:630–646, 2018. ISSN 0888-3270. doi: 10.1016/j.ymssp.2017.07.053.

[10] D. Peng, W. A. Smith, R. B. Randall, Z. Peng, and C. K. Mechefske. Speed estimation in planetary gearboxes: A method for reducing impulsive noise. *Mechanical Systems and Signal Processing*, 159: 107786, 2021. ISSN 0888-3270. doi: 10.1016/j.ymssp.2021.107786.

[11] C. Peeters, J. Antoni, Q. Leclère, T. Verstraeten, and J. Helsen. Multi-harmonic phase demodulation method for instantaneous angular speed estimation using harmonic weighting. *Mechanical Systems and Signal Processing*, 167:108533, 2022. ISSN 0888-3270. doi: 10.1016/j.ymssp.2021.108533.

[12] A. Akan and O. Karabiber Cura. Time–frequency signal processing: Today and future. *Digital Signal Processing*, 119:103216, 2021. ISSN 1051-2004. doi: 10.1016/j.dsp.2021.103216.

[13] L. Cohen. *Time-frequency analysis*, volume 778. Prentice hall New Jersey, 1995.

[14] W. Martin and P. Flandrin. Detection of changes of signal structure by using the wigner-ville spectrum. *Signal Processing*, 8(2):215–233, 1985. ISSN 0165-1684. doi: 10.1016/0165-1684(85)90075-1.

[15] I. Daubechies. The wavelet transform, time-frequency localization and signal analysis. *IEEE Transactions on Information Theory*, 36(5):961–1005, 1990. doi: 10.1109/18.57199.

[16] J. Wexler and S. Raz. Discrete gabor expansions. *Signal Processing*, 21(3):207–220, 1990. ISSN 0165-1684. doi: 10.1016/0165-1684(90)90087-F.

[17] Mallat S. Chapter 4 - time meets frequency. In *A Wavelet Tour of Signal Processing (Third Edition)*, pages 89–153. Academic Press, Boston, third edition edition, 2009. ISBN 978-0-12-374370-1. doi: 10.1016/B978-0-12-374370-1.00008-2.

[18] I. Daubechies, J. Lu, and H. Wu. Synchrosqueezed wavelet transforms: An empirical mode decomposition-like tool. *Applied and Computational Harmonic Analysis*, 30(2):243–261, 2011. ISSN 1063-5203. doi: 10.1016/j.acha.2010.08.002.

[19] Z. Li, J. Gao, H. Li, Z. Zhang, Na. Liu, and X. Zhu. Synchroextracting transform: The theory analysis and comparisons with the synchrosqueezing transform. *Signal Processing*, 166:107243, 2020. ISSN 0165-1684. doi: 10.1016/j.sigpro.2019.107243.

[20] D. Iatsenko, P. V.E. McClintock, and A. Stefanovska. Linear and synchrosqueezed time–frequency representations revisited: Overview, standards of use, resolution, reconstruction, concentration, and algorithms. *Digital Signal Processing*, 42:1–26, 2015. ISSN 1051-2004. doi: 10.1016/j.dsp.2015.03.004.

[21] D.L. Jones and R.G. Baraniuk. A simple scheme for adapting time-frequency representations. *IEEE Transactions on Signal Processing*, 42(12):3530–3535, 1994. doi: 10.1109/78.340790.

[22] R.N. Czerwinski and D.L. Jones. Adaptive short-time fourier analysis. *IEEE Signal Processing Letters*, 4 (2):42–45, 1997. doi: 10.1109/97.554468.

[23] J. Zhong and Y. Huang. Time-frequency representation based on an adaptive short-time fourier transform. *IEEE Transactions on Signal Processing*, 58(10):5118–5128, 2010. doi: 10.1109/TSP.2010.2053028.

[24] S. Meignen, M. Colominas, and D. Pham. On the use of rényi entropy for optimal window size computation in the short-time fourier transform. In *ICASSP 2020 - 2020 IEEE International Conference on Acoustics, Speech and Signal Processing (ICASSP)*, pages 5830–5834, 2020. doi: 10.1109/ICASSP40776.2020.9053392.

[25] Tsz K. Hon and A. Georgakis. Enhancing the resolution of the spectrogram based on a simple adaptation procedure. *IEEE Transactions on Signal Processing*, 60(10):5566–5571, 2012. doi: 10.1109/TSP.2012.2208637.

[26] M. Leiber, Y. Marnissi, A. Barrau, and M. Badaoui. Differentiable adaptive short-time fourier transform with respect to the window length. In *ICASSP 2023 - 2023 IEEE International Conference on Acoustics, Speech and Signal Processing (ICASSP)*, pages 1–5, 2023. doi: 10.1109/ICASSP49357.2023.10095245.

[27] N. P. Hurley and S. T. Rickard. Comparing measures of sparsity. *CoRR*, abs/0811.4706, 2008. URL `http://arxiv.org/abs/0811.4706`.